DEFORMATION ALONG HUMAN MEDIAL GASTROCNEMIUS MUSCLE FIBERS IN VIVO DURING LOW-LEVEL PLANTAR FLEXION ACTIVITY

by

Arda Arpak

B.Sc., Electrical Engineering, Sabanci University, 2010

Submitted to the Institute of Biomedical Engineering
in partial fulfillment of the requirements
for the degree of
Master of Science
in
Biomedical Engineering

Boğaziçi University
2017

ACKNOWLEDGMENTS

I would like to extend my gratitude to my thesis advisor Assoc. Prof. Dr. Can A. Yücesoy for his continual support until the completion of this work. His motivation and patience was pivotal for this work to come to fruition. I thank my thesis committee Assist. Prof. Dr. Esin Öztürk Işık and Assist.Prof.Dr. Alper Yaman for their invaluable comments. I also thank Dr. Yaman for the brief time we got to work together.

I also wish to thank my fellow workmates Uluç Pamuk and Agah Karakuzu for their friendship and hard work. Uluç's inventions demand special praise which I am happy to give. This thesis would not be possible without their contributions.

I also thank all my labmates, schoolmates, and dormmates for making Boğaziçi University a memorable experience. I would like to express my special thanks to Müge Türkaydın for her loving friendship, and for standing by me for all these years.

Lastly, I wish to thank my family for their unconditional love and support. I thank my mother for sacrificing so much of her time and energy for my sake. I thank my father for being the kind of man who will stop at nothing for my education. I express my gratitude to my sister for being my friend my entire life, and becoming my coach for this work.

This thesis was supported by grants from TUBITAK project (111E084).

ACADEMIC ETHICS AND INTEGRITY STATEMENT

I, Arda Arpak, hereby certify that I am aware of the Academic Ethics and Integrity Policy issued by the Council of Higher Education (YÖK) and I fully acknowledge all the consequences due to its violation by plagiarism or any other way.

Name :

Signature:

Date:

ABSTRACT

DEFORMATION ALONG HUMAN MEDIAL GASTROCNEMIUS MUSCLE FIBERS IN VIVO DURING LOW-LEVEL PLANTAR FLEXION ACTIVITY

Mechanical behavior of skeletal muscle has been previously shown to be determined by the interactions between contractile elements of the muscle and the extracellular matrix. Moreover, in the level of a whole limb, interactions between muscles and non-muscular structures through connective tissues have been shown to affect muscular mechanics causing varying force and movement production. The central determinant of those effects is sarcomere length changes and their heterogeneity along the muscle fibers. Quantification of that for human muscles *in vivo* is lacking. This study utilized magnetic resonance imaging (MRI) in combination with non-rigid demons image registration method to quantify local muscle tissue deformations. Additionally, diffusion tensor imaging (DTI) was used in order to determine muscle fiber direction. Combination of those methods allowed quantifying length changes along muscle fibers, *in vivo*. Presently, this method was applied to the medial gastrocnemius muscle (GM) of female subjects ($n = 4$) following a transition from 15% to 5% maximal voluntary contraction (MVC) in sustained isometric plantar flexion activity. The aim was to test the hypothesis that low-level plantar flexion activity tested results in non-uniform distribution of strain along the muscle fibers. The results show sizable simultaneous lengthening (by up to 32.7%) and shortening (by up to 15.5%) occurring along the same muscle fiber tracts. In addition, average distribution of strain across fiber tracts was also found to be heterogeneous. Therefore, the posed hypothesis was confirmed. The findings are explained through the effects of myofascial force transmission on skeletal muscle function. Insight from this work can find practical application in surgical interventions such as aponeurotomy, tendon transfer surgery, or procedures like botulinum toxin treatment.

Keywords: Diffusion tensor imaging, Magnetic resonance imaging, Tractography, Gastrocnemius, *in vivo*, Myofascial force transmission.

ÖZET

İNSAN MEDİAL GASTROKNEMİUS KASI FİBERLERİ BOYUNCA DÜŞÜK SEVİYE PLANTAR FLEKSİYON AKTİVİTESİ SIRASINDA İN VİVO DEFORMASYON

İskelet kaslarının mekanik davranışının kasın kasılabilir elemanları ile hücre dışı matrisin etkileşimine göre belirlendiği önceki çalışmalarda gösterilmişti. Dahası, tüm uzuvun ölçeğinde, bağ dokular aracılığıyla kaslar arasında ve kas dışı yapılarla etkileşimin değişken kuvvet ve hareket üretimi ile kas mekaniğini etkilediği gösterilmiştir. Bu etkilerin ana belirleyicisi sarkomer boyu değişimleri ve bunun kas fiberleri boyunca heterojenliğidir. Bunun insan kasında *in vivo* miktarının tayini eksiktir. Bu çalışmada, manyetik rezonans görüntüleme (MRG) ile demons esnek görüntü çakıştırma metodunun birleşiminden yerel kas dokusu deformasyonlarının miktarını belirlemek üzere yararlanıldı. Ek olarak, iskelet kasının fiber yönünü belirlemek üzere difüzyon tensörü görüntüleme (DTG) metodu kullanıldı. Metodların birleşimi fiberlerdeki uzama ve kısalmaların *in vivo* olarak ölçülmesine izin verdi. Bu metod kadın deneklerin ($n = 4$) medial gastrocnemius (GM) kaslarında %15'lik sürekli izometrik plantar fleksiyon maksimal istemli kasılma aktivitesinden %5 seviyesine geçişi takiben uygulandı. Çalışmanın amacı, test edilen düşük miktarda plantar fleksiyon aktivitesinin kas fiberleri boyunca homojen olmayan boy değişimleri oluşturduğu hipotezini test etmekti. Sonuçlar aynı kas fiberi traktları üzerinde eşzamanlı uzamalar (% 32,7'ye kadar) ve kısalmalar (% 15,5'e kadar) oluştuğunu göstermektedir. Ek olarak, kas fiberleri arasındaki ortalama boy değişimlerinin dağılımının heterojen olduğu gözlendi. Sunulan hipotez sonuçlar ışığında doğrulanmıştır. Bulgular miyofasyal kuvvet iletiminin iskelet kaslarının fonksiyonu üzerindeki etkileri aracılığıyla açıklanmaktadır.Bu çalışmadan elde edilen öngörüler aponevrotomi, tendon transferi ameliyatı gibi cerrahi müdahalelerde, botulinum toksin tedavisi gibi prosedürlerde pratik uygulama bulabilir.

Anahtar Sözcükler: Difüzyon tensor görüntüleme, Manyetik rezonans görüntüleme, Traktografi, Gastrocnemius, *in vivo*, Miyofasyal kuvvet aktarımı.

TABLE OF CONTENTS

LIST OF FIGURES

LIST OF TABLES

LIST OF SYMBOLS

T	Tesla
$\mathbf{G}$	Displacement gradient
$\vec{u}$	Displacement vector
$\mathbf{e}$	Green-Lagrange strain tensor
$\vec{t}$	Tract vector
S	Strain

LIST OF ABBREVIATIONS

MFT	Myofascial Force Transmission
MVC	Maximal Voluntary Contraction
SNR	Signal-to-Noise Ratio
NEX	Number of Excitations
DT	Diffusion Tensor
DTI	Diffusion Tensor Image
DWI	Diffusion Weighted Image
ROI	Region Of Interest
GAS	Gastrocnemius
GM	Medial Gastrocnemius
GL	Lateral Gastrocnemius
SOL	Soleus
TA	Tibialis Anterior
FOV	Field of View

1. INTRODUCTION

Skeletal muscles are the active components of the musculoskeletal system and animate the system by generating force. They consist of muscle fibers – the cells of the muscle, connective tissue, neural tissue, and vascular tissue. Neural tissue establish the connection of muscles to the central nervous system (CNS). This allows for voluntary activation and feedback such as fatigue. Vascular tissue is required for perfusion as with all tissues with metabolism. Muscle fibers and connective tissue require further definition pertinent to this study.

Muscle fibers contain myofibrils, the structure that is responsible for contraction. Myofibrils are considered to be a serial arrangement of a single functional unit named a sarcomere. Sarcomeres can further be broken down into thin and thick filaments, which appear as stripes under the microscope. This appearance gave rise to the alternative name striated muscle.

Sarcomere operation has been increasingly well understood in the microscopic level, since Huxley [6] and Huxley [7] described the sliding filament theory based on observations made on striated structure of the muscle. Artist's representation of the sarcomere is shown in Figure 1.1. The region between two Z-lines (Z-disks) is repeated to form the myofibril. Thick and thin filaments are protein structures named myosin and actin proteins, respectively. Actin proteins are anchored to Z-discs, myosin proteins are located overlapping with actin filaments. Other proteins inside the cell, such as titin, nebulin, α-actinin, tropomyosin, help facilitate and stabilize the sarcomere operation.

Upon neural activation, myosin filaments spend chemical energy in form of ATP to slide over the actin filaments and bring the Z-discs closer together, thus shortening the system. Operation does not work the other way though, elongation is always due to external forces. The amount of overlap between actin and myosin filaments is the

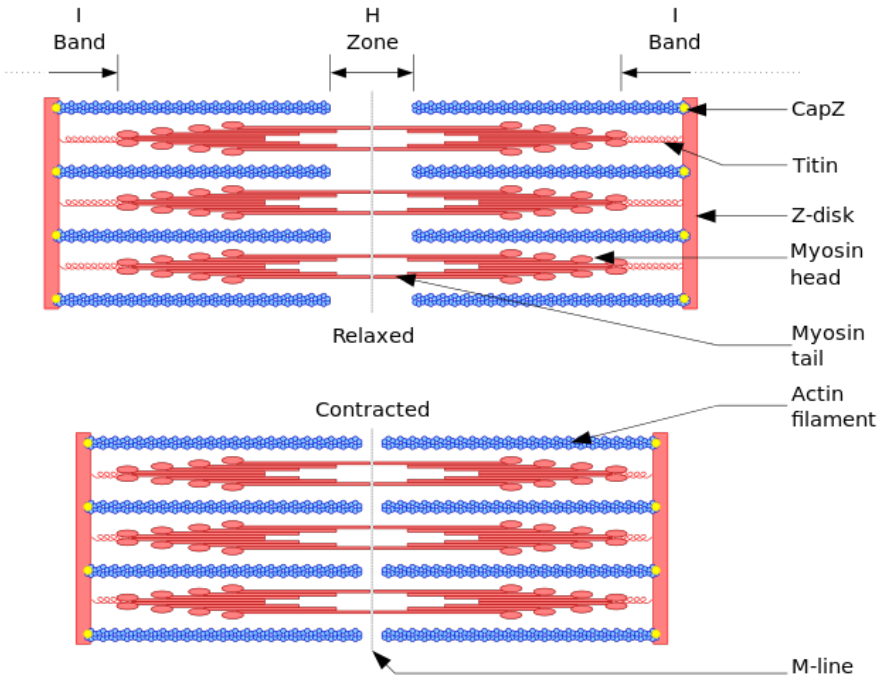

Figure 1.1 Model of the sarcomere [1].

determinant of active force generated by the sarcomere. Sarcomeres are certainly the source of muscular contraction, however, it is not possible to merely summarize the muscle as a population of sarcomeres. Connective tissue in the muscle rather plays an important role in collective operation and interaction of sarcomeres.

In order to better understand the complex collective behavior of the muscle, one needs to look at the complex hierarchy of the muscular structure. Muscle fibers encapsulate a bundle of myofibrils with sarcolemma. Neighboring myofibrils are mechanically connected to each other and sarcolemma, which in turn is connected to the endomysium, forming a tubular structure for the myofibrils to operate in. Endomysial tunnels are so well connected that they can be considered to form a singular structure named the extracellular matrix (ECM). This structure is encapsulated by perimysium, forming fascicles. Finally, fascicles are enveloped by the epimysium at the periphery of the muscle (see Figure 1.2). Connective tissue extend beyond the muscle belly forming a tendon or aponeurosis. Tendons terminate at a bone typically after passing a joint. The muscle's epimysium also have collagenous connections to neighboring muscles through structures like neurovascular bundles, extending mechanical connections

of connective tissue beyond the epimysium.

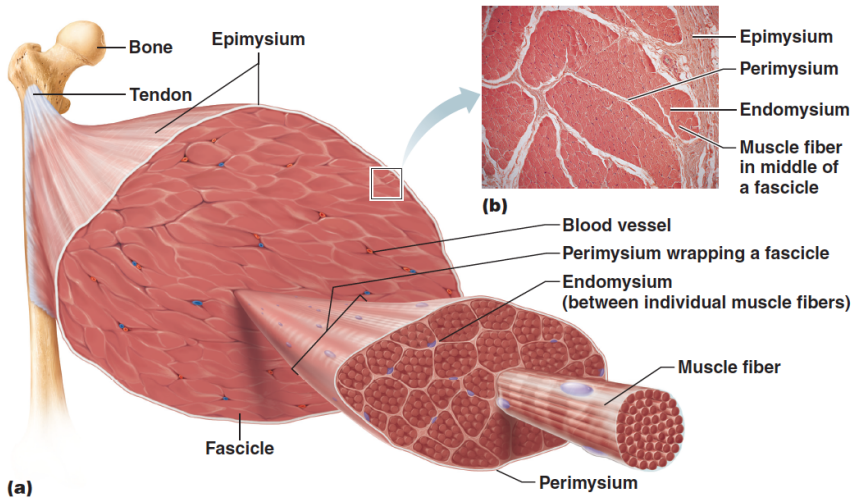

Figure 1.2 Hierarchical structure of the muscle [2].

It is often considered that tendons are the primary isolated tissues that are responsible for transferring forces generated by muscle to the rest of the system. Although tendons are elements specialized in force transfer, they are not the sole determinants of it: for instance, (i) Skeletal muscle is also capable of distributing force across its direction of fibrosity through its internal elastic and structural network [8, 9]. This mechanism is referred to as intramuscular myofascial force transmission (MFT) [10] . (ii) Muscle is mechanically linked to neighboring muscles through collagenous links as well as through non-muscular tissues – e.g. collagen reinforced structures enveloping nerves and blood vessels (neurovascular tracts). This mechanism is referred to as epimuscular myofascial force transmission (EMFT) [11, 12, 13, 14]. In other words, muscular force transmission mechanisms are not restricted by the "boundaries" of the muscle belly, but large quantities of muscle forces can be also transmitted via muscle related connective tissues.

Connections between different groups of muscles (epimuscular) and connections between components of a muscle (intramuscular) both affect muscle operation. Huijing et al. [12] imposed equal proximal and distal lengthening on rat extensor digitorum longus (EDL) while keeping connective tissues around the muscle intact. Forces mea-

sured at proximal and distal tendons were shown to be unequal. Active force-length relationship of the muscle varied based on its position relative to its surrounding structures. This shows that obtained length-force values under one condition cannot be utilized to extrapolate or to predict possible length-force values in other conditions. That is, the length-force relationship of the muscle cannot be taken to be a constant – a unique property – under all conditions.

In another study [15], a finite element model of the muscle was used to model muscular dystrophy. Muscular dystrophy occurs due to the lack of dystrophin, a cytoplasmic protein that binds the cytoskeleton to surrounding extracellular matrix. In order to replicate the deficiency of dystrophin in the model, stiffness of the connections between myofibrils and extracellular matrix were reduced. Muscle operation was altered – damaged – significantly, when intramuscular strain distribution was modified by weakening the connections. Similar results were obtained both in simulations and aponeurotomy application on rats [16].

These results contribute to inquiry that some of the inherent assumptions in classical models may have been rather too simplified or reductionist. Strain distribution in the muscle is indeed non-uniform [15, 16]. Therefore, we need to better grasp the epimuscular and intramuscular connections that contribute to this non-uniformity. Skeletal muscle will present various strain patterns on it even at a singular muscle length, according to changes in its surroundings. Thus, resulting in situations like varying maximal forces and optimal muscle lengths of a muscle. Yet, this problem is often overlooked by agglomerating muscle behavior to a characteristic model and assuming no behavioral change in different mechanical configurations. Moreover, it is not known well if the previously theoretically shown non-uniform strain distributions are relevant for human muscles in vivo.

In this thesis, we propose one way to approach this problem by combining strain analysis and fiber tractography techniques in order to derive strain distribution in the fiber direction of human medial gastrocnemius muscle (GM) *in vivo* (Figure 1.3). Data gathered from two different levels of activation of the same muscle helps

us evaluate the significance of myofascial force transmission (for technical results in isometric contractions, see [17]). In this work, we examined two levels of contraction of GM at 15% and 5% isometric maximal voluntary contraction (MVC). We gathered T1 weighted 3-D images of the lower leg in magnetic resonance image scanner (MRI). Using the acquired images we calculated strain fields by applying the demons algorithm method [18]. Therefore, although we do not measure force directly, we aim at inferring the effects of it by elaborating on deformations in tissue in a unique way.

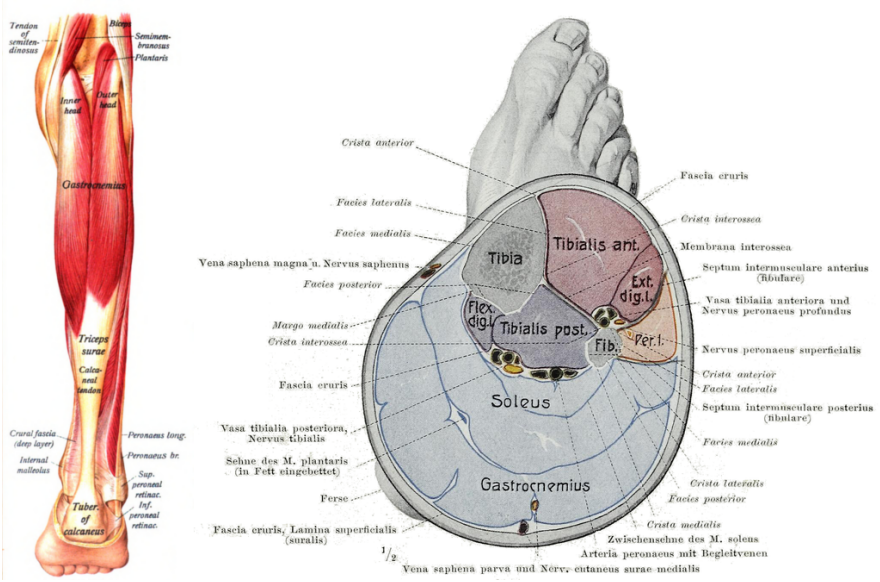

Figure 1.3 The gastrocnemius muscle as seen from the posterior [3] and on an axial slice [4].

While applying the strain analysis method, we also performed fiber tractography techniques. Fiber tractography technique gave us information about the orientation of muscle fibers, and based on this the orientation of myofibrils, within the local muscle volume studied. Previous studies [17] observed strain in active muscle and found simultaneous positive and negative length changes. However, they did not examine or determine whether or not positive and negative length changes were in fact along the same fibers of the muscle. Pennation angle of GM is of importance to make physiologically relevant observations and interpretation of the strain data. Sarcomere length is directly connected to force generation of the skeletal muscle. Therefore, seeing changes in sarcomere length in a direct manner makes it possible for us to make judgments about the force generation function of the active muscle.

In light of this background, the aim of this thesis was to test the hypothesis that sustained low-level plantar flexion activity causes heterogeneous strain distributions along the muscle fibers of the human GM, *in vivo*.

2. METHODS

The purpose of this study was to observe changes in GM fiber length in a direct manner in order to make judgments on the force generation function of the active muscle. In approaching this problem, we combined strain analysis and fiber tractography techniques in order to derive distribution of changes in length in the fiber direction of human GM, *in vivo*.

Experiments were conducted on four subjects. Prior to the imaging study, force that was exerted by each subject while performing isometric MVC during plantar flexion effort was measured. Then, subjects were placed inside an MRI scanner. Their feet were strapped to a custom built foot pedal mounted with an MRI-compatible strain gauge. Subjects performed sustained 15% and 5% MVC isometric plantar flexion. High resolution anatomical images and diffusion tensor images (DTI) of the lower leg were acquired at this time.

Strain tensor data was derived from the high resolution images by applying demons non-rigid image registration [18]. Skeletal muscle fibers were tracked by applying fiber tractography technique on the DTI image set [19]. Fiber tracts gave us information about the orientation of muscle fibers within the muscle volume studied. Strain information was then mapped on the derived tracts in order to observe changes in fiber tract length. Fiber tract lengthenings and shortenings were studied by statistical tools and visually reconstructed in 3-D. Although spatial resolution limitations of employed MRI sequences, combined strain and fiber direction information allowed us to make physiologically relevant observations and interpretations.

2.1 Subjects

Experimental procedures were in strict agreement with the guidelines and regulations concerning human welfare and experimentation set by Turkish law and approved

by a Committee on Ethics of Human Experimentation at Bogazici University, Istanbul. Four female subjects volunteered for this study. All subjects were non-athletes and all reported a clean bill of musculoskeletal health. Subjects were selected to be exclusively female to minimize absolute inter-subject anthropometric differences. Following a detailed explanation of the purpose and methodology of the experiments, subjects gave their written informed consent. Physical information of the subjects are presented at Table 2.1.

Table 2.1
Anthropometric data for the subjects.

Subject	Height (cm)	Weight (kg)	Age	Knee extension (°)
A	160	47	25	178
B	154	45	27	176
C	160	52	29	176
D	165	56	28	178

2.2 Experimental Protocol

Experimental setups, devices used, MRI sequences and post processing steps are detailed in this section.

2.2.1 Maximal Voluntary Contraction Measurement

All subjects' individual isometric MVC during plantar flexion were measured. Subjects were placed on a table in prone position. Right foot was put on a custom built force measuring pedal (Figure 2.1), such that the knee joint was maximally extended and ankle angle was 90°. Pedal was equipped with a strain gauge to measure the force exerted by the subject. Foot was firmly fastened to pedal's base in order to maintain ankle angle without activation of dorsiflexor muscles. Pre-gelled, self adhesive electromyography (EMG) surface electrodes were applied on the lower leg to

collect muscle activation data from tibialis anterior (TA), soleus (SOL), GM, and lateral gastrocnemius (GL) during subject's plantar flexion effort (Biopac MP150 with DA100C, CA, USA). Note that all strain gauges used in this study were calibrated using precision calibration weights.

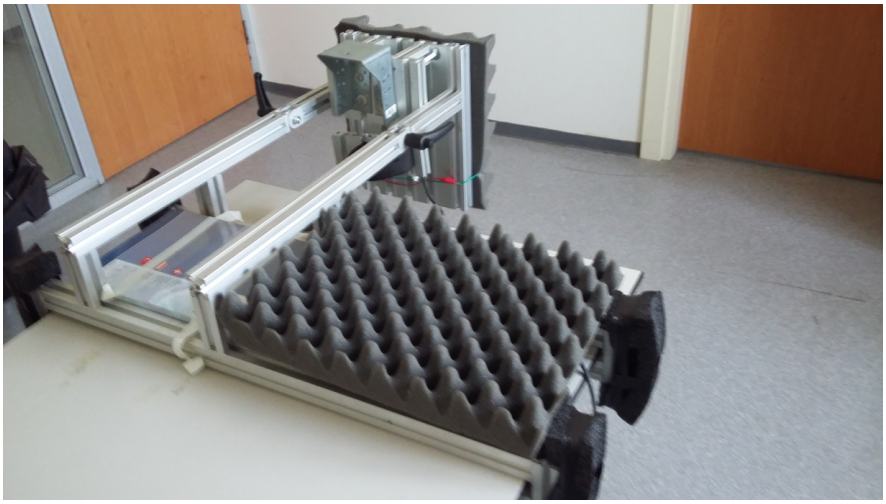

Figure 2.1 Force measurement pedal used in determining MVC.

Subjects were asked to push the pedal with maximum effort and maintain the push for five seconds. This was repeated minimum of three times with two minute rest periods in between. If the force between tries varied less than 5%, largest reading was taken to be the MVC in plantar flexion for the subject. Otherwise, additional maximal efforts were performed until the variation became less than 5%. Subjects were then trained to exert and sustain isometric 15% and 5% MVC for six minutes with the help of visual feedback; same visual feedback to be used during MRI data acquisition. Six minutes was selected because it is the approximate time for the MRI sequences used.

2.2.2 Image Acquisition in MRI

Subjects were placed inside a 3T full body MR scanner (Siemens Magnetom Trio, Erlangen, Germany) in prone position, feet first. Right foot was put in a pedal and fastened to its base, such that the knee joint was fully extended ($177° \pm 1°$) and ankle angle was 90°. Pedal was made of MRI compatible material, and was equipped with a

strain gauge, also MRI compatible. A piece of Velcro was attached over the patella to anchor the knee joint on the MRI table, thus immobilizing the knee. Care was taken not to exert external loads on the muscles and tendons of interest. MVC percentage data was fed to the subject in real time from an MRI compatible monitor (Telemed, Istanbul, Turkey). Feedback allowed the subjects maintain 15% and 5% MVC plantar flexion during data acquisition. Imaging study was performed in Kozyatagi Acibadem Hastanesi, Istanbul.

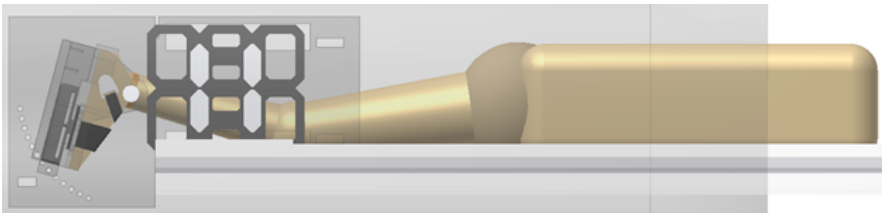

Figure 2.2 Positioning of the subject and the strain gauge mounted force measurement pedal inside the MRI bore.

Two 6-channel surface coils were mounted on either side of the pedal, at the region corresponding to the lower leg (Figure 2.2). Anatomical images were obtained using a 3D turbo fast - low angle shot (3D Turbo FLASH) sequence. Field of view (FOV) was selected to be between most proximal part of the head of tibia and most proximal part of the transverse crural ligament. Slice orientation was coronal, proximo-distal direction was frequency encoded, and left-right direction was phase encoded. Left leg was also placed inside the FOV in order to avoid aliasing artifacts as it was in phase encoding direction. A high bandwidth was selected to minimize chemical shifting artifacts.

DTI data was acquired using single-shot echo planar imaging (ss-EPI) based multi-directional sequence. 2D planar slice selection was done axially. FOV was selected to begin at proximal neck of tibia and extend along longitudinal axis the size of axial image stack (112 millimeters, Figure 2.3). Fat suppression excitation was performed and frequency encoding direction was selected to be posterior-anterior direction to keep the chemical shift artifacts outside gastrocnemius (GAS) muscles. Reader may refer to Table 2.2 for anatomical MRI and DTI sequence parameters.

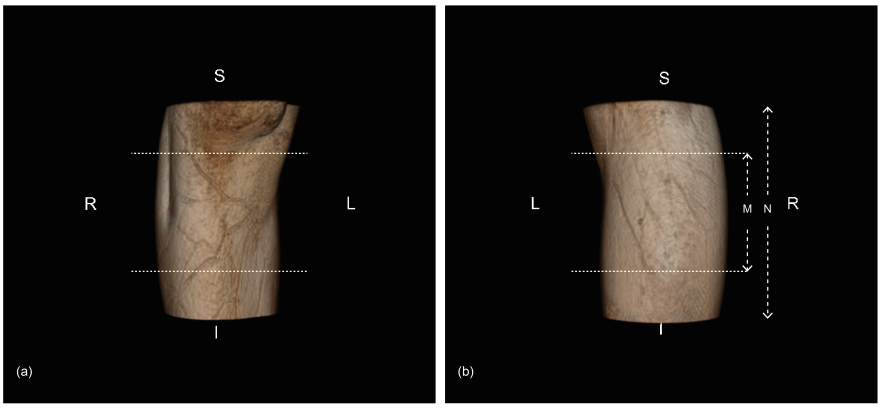

Figure 2.3 3-D reconstruction of the lower leg in (a) anterior view (b) posterior view. (M) is the volume imaged by DTI sequence (N) is the volume strain analysis was applied on.

Anatomical and DTI data were collected for two states of each subject. Images were acquired at isometric 15% MVC plantar flexion as the reference undeformed state; the process was repeated at isometric 5% MVC plantar flexion as the deformed state.

2.2.3 Determination of DTI Parameters

Determining the specific parameters to be used during the DTI study required striking a balance between the image quality and the imaging duration. Imaging duration required to be short, in order to ensure that the subjects could sustain a stable level of contraction. On the other hand, image quality was directly proportional to the time spent during acquisition. The ultimate goal of DTI image acquisition was performing fiber tractography. Metrics used by tractography (e.g. fractional anisotropy (FA)) were reported to require a high signal-to-noise ratio (SNR) level [20]. Thus, SNR was set as the primary determinant of image quality.

A number of parameters were required to be considered in order to successfully get the desired data. For instance, a FOV containing the region-of-interest (ROI) was to be selected. However, FOV size was limited by time constraints – a larger volume required longer time – as well as by the effects of magnetic field inhomogeneity [21]. A b-value suitable for the muscle tissue was selected from the range confined by the

literature [22, 23, 24], and after performing trials at two different b-values. Table 2.2 summarizes eight trials performed in order to determine the optimal parameters that would yield the highest SNR. Single image SNR was calculated from the b0 magnitude image of a single excitation using the eq. 2.1 as defined by Henkelman [25].

$$SNR = 0.655 \times \frac{average\ signal\ at\ ROI}{std.\ dev.\ of\ background} \tag{2.1}$$

The number of excitations (NEX) improved the effective SNR by accumulating the signal from different repetitions. As a result, parameters for Trial-5 was elected to be used in the actual imaging study.

Table 2.2
Anatomical MRI and DTI sequence parameters.

	Trial-1	Trial-2	Trial-3	Trial-4	**Trial-5**	Trial-6	Trial-7	Trial-8	MRI
Slice orientation	Axial	Axial	Axial	Axial	Axial	Axial	Axial	Axial	Coronal
Number of gradients	20	20	12	12	12	12	12	12	-
b-value (s/mm^2)	600	600	450	450	450	450	450	450	-
FOV (mm^2)	192×192	192×192	192×192	180×180	180×180	180×180	192×192	192×192	320×320
Matrix size	96×96	96×96	128×128	64×64	64×64	90×90	96×96	96×96	320×320
Number of slices	50	25	40	30	30	47	50	50	128
Slice thickness (mm)	2	4	2	2.8	2.8	2	2	2	1
Voxel size(mm^3)	2×2×2	2×2×4	1.5×1.5×2	2.8×2.8×2.8	2.8×2.8×2.8	2×2×2	2×2×2	2×2×2	1×1×1
Repetition time (TR)(ms)	8000	3600	5100	3700	3700	5800	6100	6100	1750
Echo time (TE)(ms)	110	97	81	61	61	69	70	73	3.36
Flip angle (°)	90	90	90	90	90	90	90	90	12
Bandwidth (Hz/pixel)	-	-	1184	2003	2003	1984	2003	2003	130
NEX	1	1	1	1	8	8	8	8	1
Fat supression	Fat Sat.	Fat Sat.	Fat Sat.	Fat Sat.	Fat Sat.	Fat Sat.	Fat Sat.	Fat Sat.	no
Phase encoding direction	A»P	A»P	A»P	A»P	A»P	A»P	A»P	A»P	-
Parallel imaging	GRAPPA	GRAPPA	GRAPPA	no	no	no	no	no	no
Phase partial Fourier	8/8	8/8	8/8	5/8	5/8	5/8	5/8	5/8	8/8
Acquisition time (mm:ss)	03:14	01:28	02:20	00:53	06:26	07:36	10:36	10:35	06:06
Single image SNR	6	10	3	14	14	6	6	8	130
Effective SNR	6	10	4	14	40	15	17	23	130

2.3 Post-Processing

Images contain information on morphological change of lower leg structures, and orientation of anisotropic structures like nerves, veins and muscle fibers. It is necessary to calculate and isolate the information of interest through mathematical means.

2.3.1 Derivation of Strain

2.3.1.1 Quantification of Displacement Field. Displacement field is a set of vectors defining each voxel's change of position in space to have arrived its position in the deformed state form the undeformed state. A non-rigid, non-parametric image registration algorithm treating image matching as a diffusion process named demons algorithm [18] is employed to derive the displacement field information. The algorithm accepts two images as input, one static and one moving, and outputs the displacement field (Figure 2.4). The algorithm iteratively approximates one image to the other using a strategy analogous to diffusion. To this end, the algorithm computes a difference image between static and moving image and divides them with the image intensity gradients in the static image. When the image intensity gradient becomes too small, a computational error arises because small numbers in the denominator cause displacement vectors to have infinite value, thus leading to instability. This is overcome by introducing a smoothing Gaussian kernel between each iteration, until convergence is achieved based on set criterion.

Anatomical images and DTI both represent a sub-section of the same subject. Since the subject is not re-positioned between acquisitions, two images overlap at the ROI of the right lower leg in the physical domain. However, differences in acquisition schemes, resolutions and FOV cause the images to differ in their image domains. To overcome inconsistencies, anatomical image direction conventions were matched to DTI's. Followed by removing the superfluous data (e.g. left leg) in the anatomical image; leaving 32mm buffers above the proximal and below the distal boundary of the region corresponding to the DTI. Buffer zones allow for boundary artifacts produced

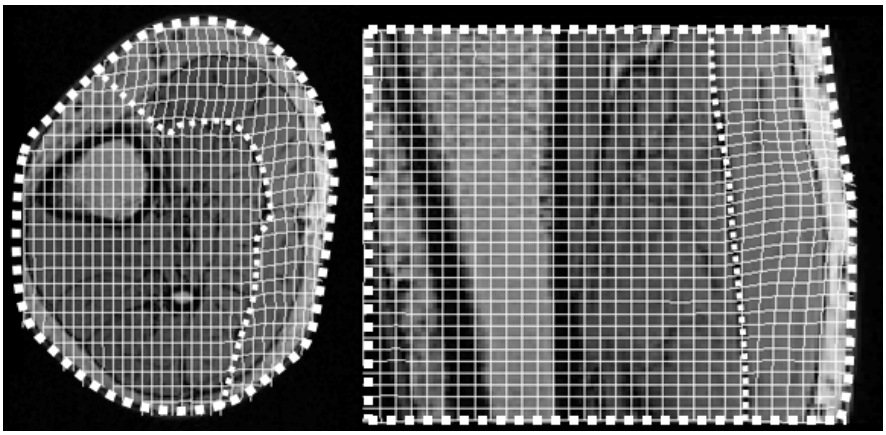

Figure 2.4 Calculated deformation field is masked to GM muscle and applied on a grid. Grid is then superimposed on axial (left) and sagittal (right) GM slice views [5].

by demons algorithm to subside. Subsequently, demons registration was performed on the anatomical images between undeformed and deformed states in MATLAB R2012a (The Mathworks Inc., Natick, MA).

Demons registration outputs the displacement field as mapped to the undeformed state. That is, a displacement vector defines a grid point in the undeformed image moving an arbitrary amount to reach its new position in the deformed state, not necessarily landing at a point on the deformed state image grid. However, our subsequent analysis steps require the displacement field to conform to said grid. To achieve this, displacement vectors were transformed to their corresponding grid positions in the deformed state.

2.3.1.2 Quantification of Strain Tensors. Differences in displacement of adjacent voxels constitute the basis of strain. One can intuitively see if neighboring voxels move further away from each other, lengthening will occur. Conversely, if voxels move closer together, underlying structure will have shortened. In three dimensional space, in order to express the full change in displacement, a 3-by-3 Jacobian matrix is needed. This matrix is termed a displacement gradient ($\mathbf{G}$), and can be expressed as follows (Eq. 2.2).

$$\nabla \vec{u} = \begin{bmatrix} \frac{\partial u_x}{\partial X} & \frac{\partial u_x}{\partial Y} & \frac{\partial u_x}{\partial Z} \\ \frac{\partial u_y}{\partial X} & \frac{\partial u_y}{\partial Y} & \frac{\partial u_y}{\partial Z} \\ \frac{\partial u_z}{\partial X} & \frac{\partial u_z}{\partial Y} & \frac{\partial u_z}{\partial Z} \end{bmatrix} = \mathbf{G} \tag{2.2}$$

where $\vec{u} = [u_x, u_y, u_z]$ is the displacement vector. A suitable measure for finite strain is the Green-Lagrange strain tensor ($\mathbf{e}$), defined as:

$$\mathbf{e} = \frac{1}{2}\left(\mathbf{G} + \mathbf{G}^T\right) + \frac{1}{2}\mathbf{G}^T\mathbf{G} \tag{2.3}$$

where $\mathbf{e}$ is a 3-by-3 symmetrical matrix.

2.3.2 Muscle Fiber Tractography

Diffusion tensor tractography is a post-processing technique applied on the DTI data in order to detect configuration of tubular structures (tracts) inside the tissue of interest *in vivo* [26]. Tissue type and tract direction are inferred by making use of anisotropic diffusion of the water molecules. 3-D reconstruction of tracts allows us to visualize connectivity information at the macro scale that otherwise would be confined to single voxels.

MRI images are afflicted with Rician noise. It is imperative to apply noise reduction on diffusion weighted images (DWI) before applying diffusion tensor estimation [27]. Rician noise reduction was also shown to improve fiber orientation estimation [28]. In this study, DWI were de-noised using a joint information noise reduction algorithm. Joint information here means that images of the same slice but with different diffusion vectors are utilized in calculating noise estimation. Level estimation for the noise was performed using linear minimum mean square error estimator in MATLAB R2012a

(The Mathworks Inc., Natick, MA) [29].

A modified version of the VAV frame^{TM} software was used (VAVlab, Istanbul, Turkey) [30, 31]) in order to perform muscle fiber tractography. Firstly, de-noised DWI were used to perform diffusion tensor (DT) estimation for each voxel. From DTs, fractional anisotropy (FA) parameters were calculated. Seed points were selected from the voxels having a minimum FA of 0.1 [32]. Seed points were tracked bidirectionally following the principal diffusion direction of the DT. Half of the smallest voxel dimension was used as the step size, *i.e.* 0.7 mm [33]. At points corresponding to non-integer points on the image grid, Log-Euclidian framework was used for DT interpolation. Tracts were terminated if FA was greater than 0.5 or curvature per step exceeded 5°. Also, tracts were confined between 30-50 mm of length in order to adhere with GM muscle geometry [34]. Muscle tract reconstruction was carried out using a 4th order Runge-Kutta streamline integration algorithm [35].

Muscle fiber tractography process yielded a set of tracts as its result. However, despite set termination conditions, limitations in resolution and noise suppression still allowed the algorithm to surpass tissue boundaries. For instance, some tracts were found to traverse neighboring muscles and aponeurosis. Additional elimination steps were employed in order to filter out extraneous tracts. Two ROI masks were prepared on axial slices. Only the fibers passing through both ROIs were kept. Fibers extended outside GM anatomical boundaries and fibers that do not comply with GM pennation angle range were also manually extracted from the fiber set. Resulting fibers were found to be representative of the GM muscle (Figure 2.5).

2.3.3 Combining Fiber Tracts with Strain

Strain in fiber direction is physiologically relevant information as it pertains to sarcomere length changes. It is derived by combining strain tensor data with fiber tract data [36]. Operation involves the local strain tensor and the unit tract vector. Unit tract vector is the vector with magnitude of one that represents the local direction of

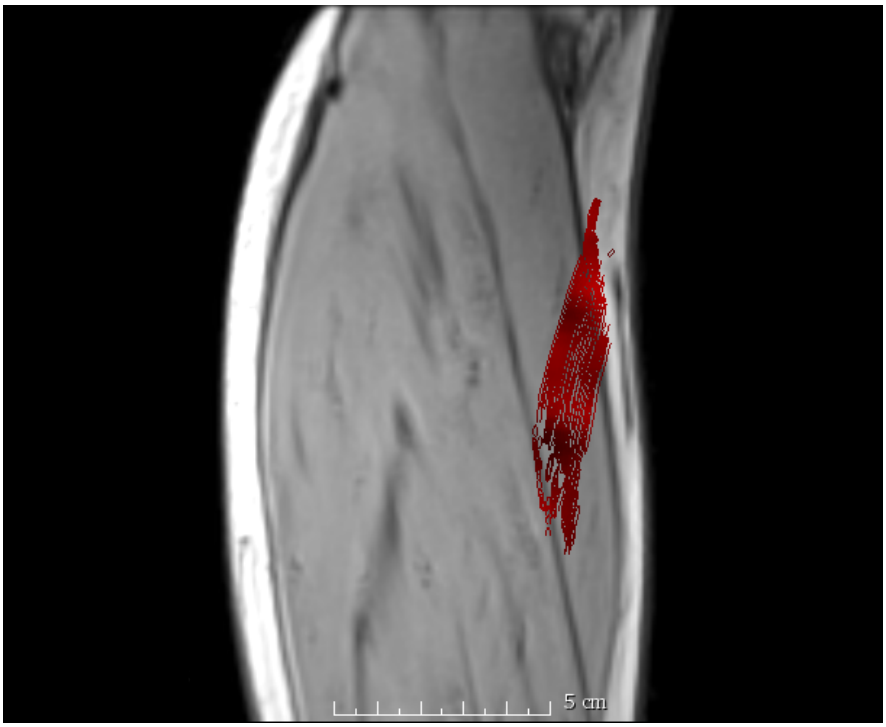

Figure 2.5 GM fiber tracts in coronal view. Pennation angle is in agreement with previous anatomical knowledge and hinted fiber angles in the image.

a given tract in 3-D space. It is numerically obtained by subtracting neighboring tract nodes' position vectors and normalizing its magnitude; denoted as $\vec{t}$. Magnitude of strain in tract direction is extracted from strain tensor using the Eq. 2.4.

$$S_{fiber} = \vec{t}^{T}\mathbf{e}\vec{t} \tag{2.4}$$

where S_{fiber} is the scalar value representing the magnitude of strain. Strain information is only readily available on anatomical image grid points. Tracts, however are not constrained by the image grid. Hence, strain tensor was estimated via linear interpolation in off-grid points of tracts.

2.3.4 Visualization of Strain Along Tracts

Fiber tracts and their corresponding fiber direction strain information were transferred into 3D Slicer software [37]. Reconstructed muscle fiber tracts were visualized and strain information was color coded onto the tracts using tractography display module of 3D Slicer.

2.3.5 Estimation of Errors

Synthetic rigid body motion was imposed on the undeformed state anatomical image. In order to obtain the synthetically generated image, the following operations were performed on the undeformed state anatomical image: 10° rotation about the axial plane, 3° rotation about the sagittal and coronal planes, 4 mm axial rotation. Original and generated image pair were fed to the data processing pipeline. Since the modifications are entirely rigid – only rigid transformations of rotation and translation in 3-dimensional space – the amount of deformation should theoretically be zero. However, in practice, resampling and demons algorithm cause minor deviations from zero which we take to be our error estimate (see the box plots in Figure 3.1).

2.3.6 Statistics

Non-parametric Wilcoxon rank-sum tests were performed on fiber direction strains vs. fiber direction error strains to evaluate the statistical significance of the results. Lengthening and shortening were tested separately. Significance level was set to be $p < 0.05$.

3. RESULTS

The difference between mean error lengthening (1±1%) and shortening (2±3%), and mean fiber direction lengthening ($3 \pm 2\%$) and shortening ($4 \pm 2\%$) were found to be statistically significant resulting from a decrease in MVC from 15% to 5% (Figure 3.1a).

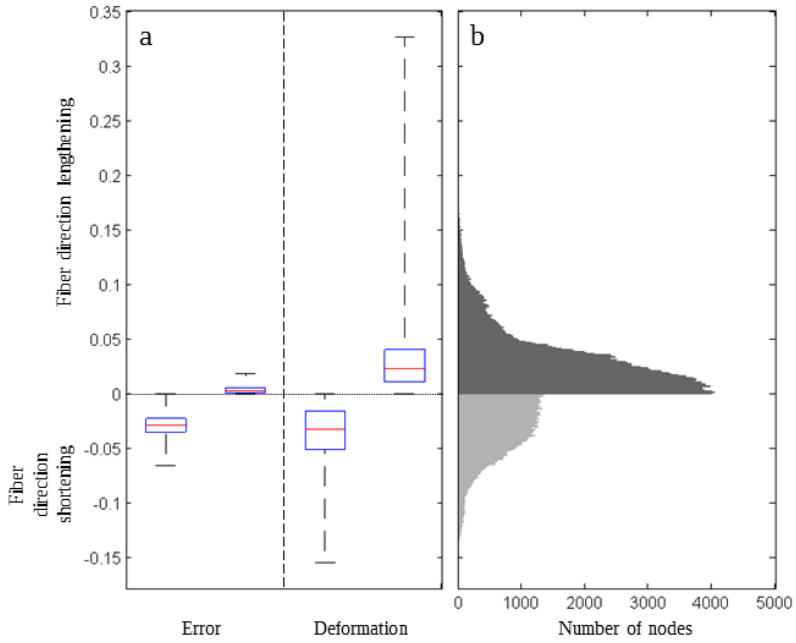

Figure 3.1 (A) Left block: strain error levels. Right block: strain measurements due to lowered muscle activation. Box-and-whisker plots showing distribution of local lengthening and shortenings in fiber direction of GM, due to transition from 15% MVC to 5% MVC isometric plantar flexion. Data belonging to fibers from all subjects are pooled. Horizontal red line inside the box marks the median value, blue solid box indicates the IQR, dashed lines (whiskers) extend to show the peak values.(B) Distribution of strain data pooled from all subjects represented as a bar graph.

3.1 Fiber Direction Strain in Medial Gastrocnemius

Pooled data (Figure 3.1) and 3D representation of fibers per subject (Figures 3.2 to 3.5) show a serial distribution of strain along muscle fibers. Due to lack of joint

angle changes, global muscle length remained constant. Local length changes along the tracked muscle fibers were possible though, and that is what we observed. Simultaneously occurring local lengthening and shortening along GM fascicles are present at different locations. A general pattern observed across subjects is a pronounced fiber direction lengthening close to GM's insertion to its distal aponeurosis.

It is interesting to note that while the distal end of the GM lengthened, same fibers exhibit less pronounced lengthening and even shortening toward muscle belly and proximal tendon region. Inter-subject variability was nevertheless sizable. Pronounced lengthening (by up to 32.7%) is toward most medial part of GM for Subject-A (Figure 3.2), whereas this is more centered for other subjects. Subject-A also solely presents a concentrated local lengthening at central-proximal region of the GM at its connection to the proximal tendon. Lesser length changes appear distributed, albeit not homogeneous. Muscle fiber tracts of Subject-A and Subject-D (Figure 3.5) both have their maximal shortening (by 15.5% for Subject-A and 10.9% for Subject-D) adjacent to the maximally lengthened region. However, muscle fibers of Subject-B (Figure 3.3) and Subject-C (Figure 3.4) show maximal shortening (by 7.0% for Subject-B and 10.3% for Subject-C) at the proximal end of the muscle.

Table 3.1
Statistical summary of strain values along fiber direction, belonging to each subject and with all fibers pooled. (+) indicates lengthening, (-) indicates shortening.

Subject	A	B	C	D	Pooled
Max. lengthening	32.7%	11.8%	10.3%	11.6%	32.7%
Max. shortening	15.5%	10.9%	7.0%	13.8%	15.5%
Mean lengthening	4.7%	2.8%	2.5%	2.8%	3.0%
Mean shortening	3.8%	3.9%	2.4%	4.5%	3.9%
Mean	0.7(+)%	1.6(-)%	0.1(+)%	2.2(-)%	1.0(-)%
Median	0.4(+)%	1.9(-)%	0.2(+)%	2.3(-)%	1.0(-)%
IQR	7.0%	5.8%	4.1%	6.2%	5.8%

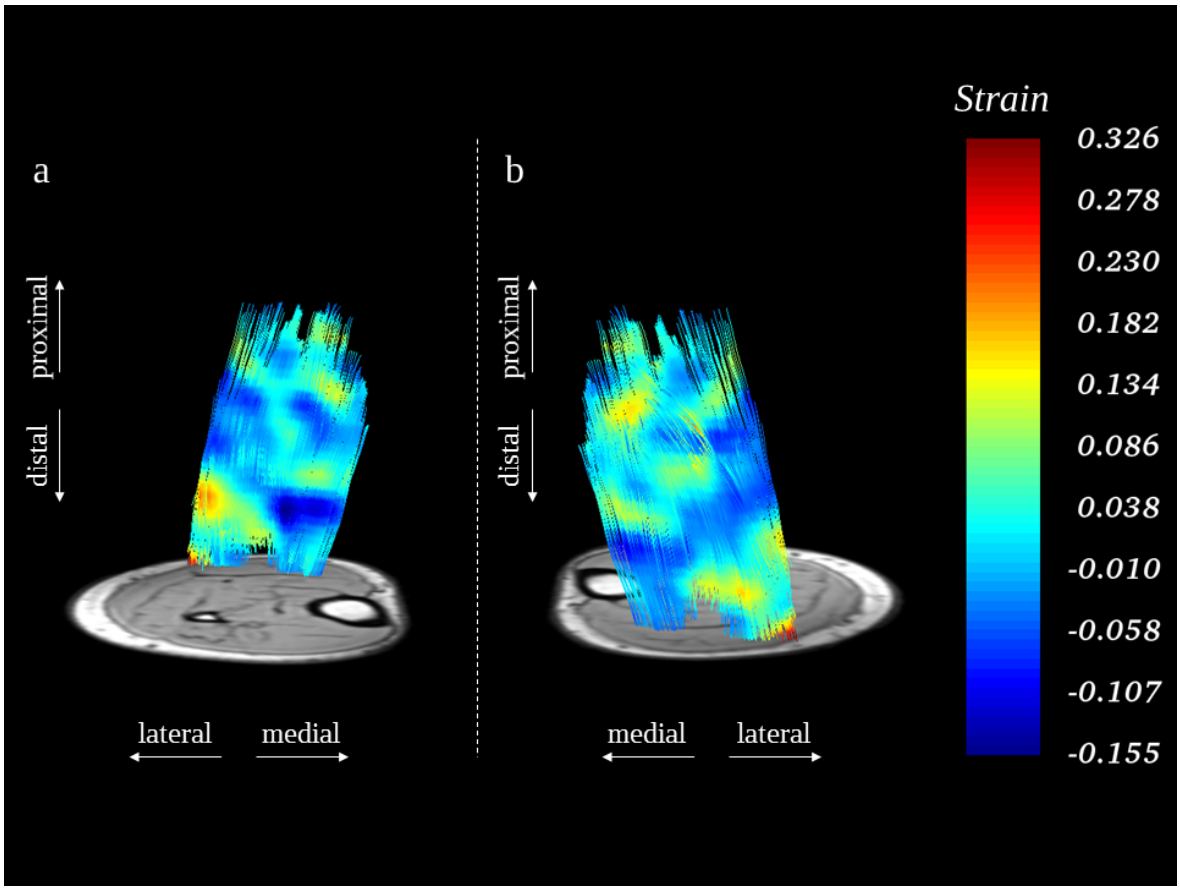

Figure 3.2 3D visualization of the reconstructed GM tracts for Subject-A. Tracts are color coded to represent deformation strain measured due to transition from 15% MVC to 5% MVC isometric plantar flexion. (a) Anterior-lateral view. (b) Posterior-medial view. Colorbar enumerates fiber direction strain presented on the tracts. Positive strain indicates lengthening, negative strain indicates shortening w.r.t. undeformed state.

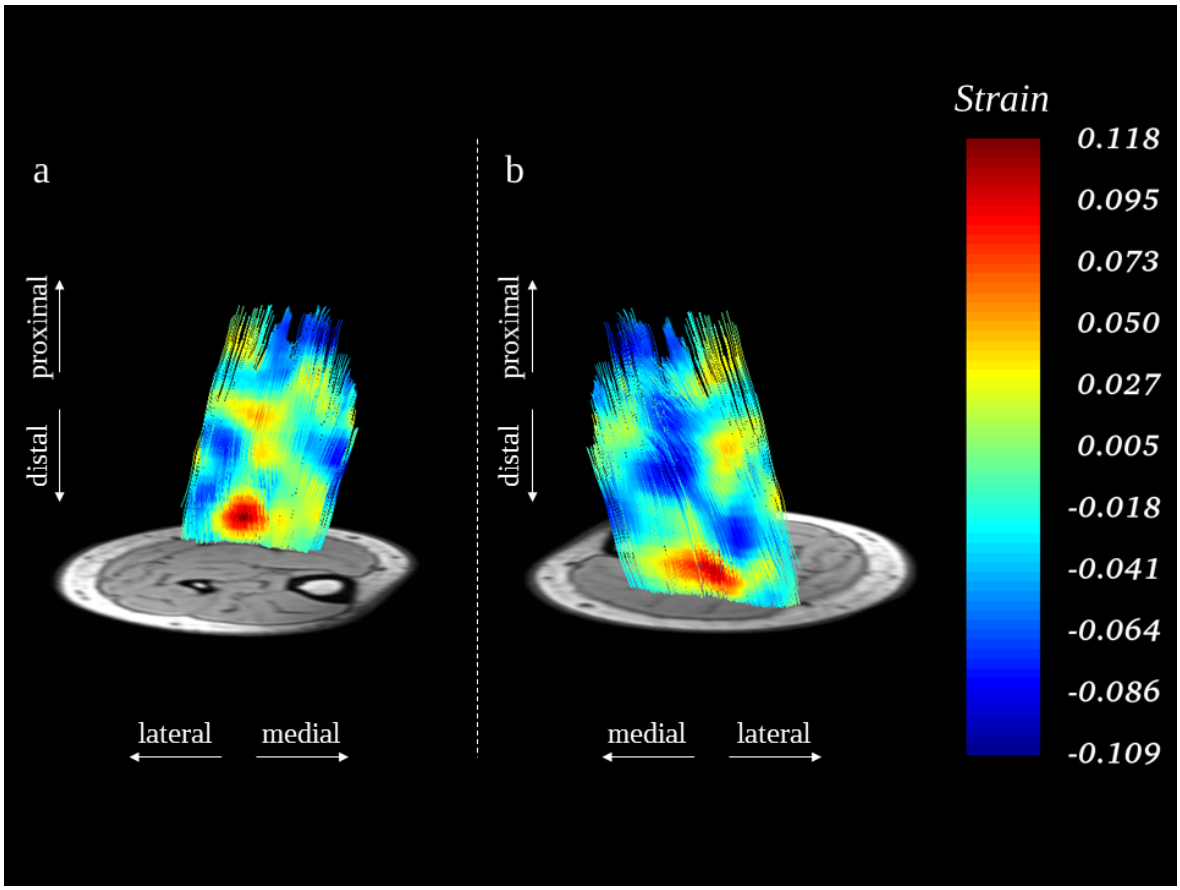

Figure 3.3 3D visualization of the reconstructed GM tracts for Subject-B. Tracts are color coded to represent deformation strain measured due to transition from 15% MVC to 5% MVC isometric plantar flexion. (a) Anterior-lateral view. (b) Posterior-medial view. Colorbar enumerates fiber direction strain presented on the tracts. Positive strain indicates lengthening, negative strain indicates shortening w.r.t. undeformed state.

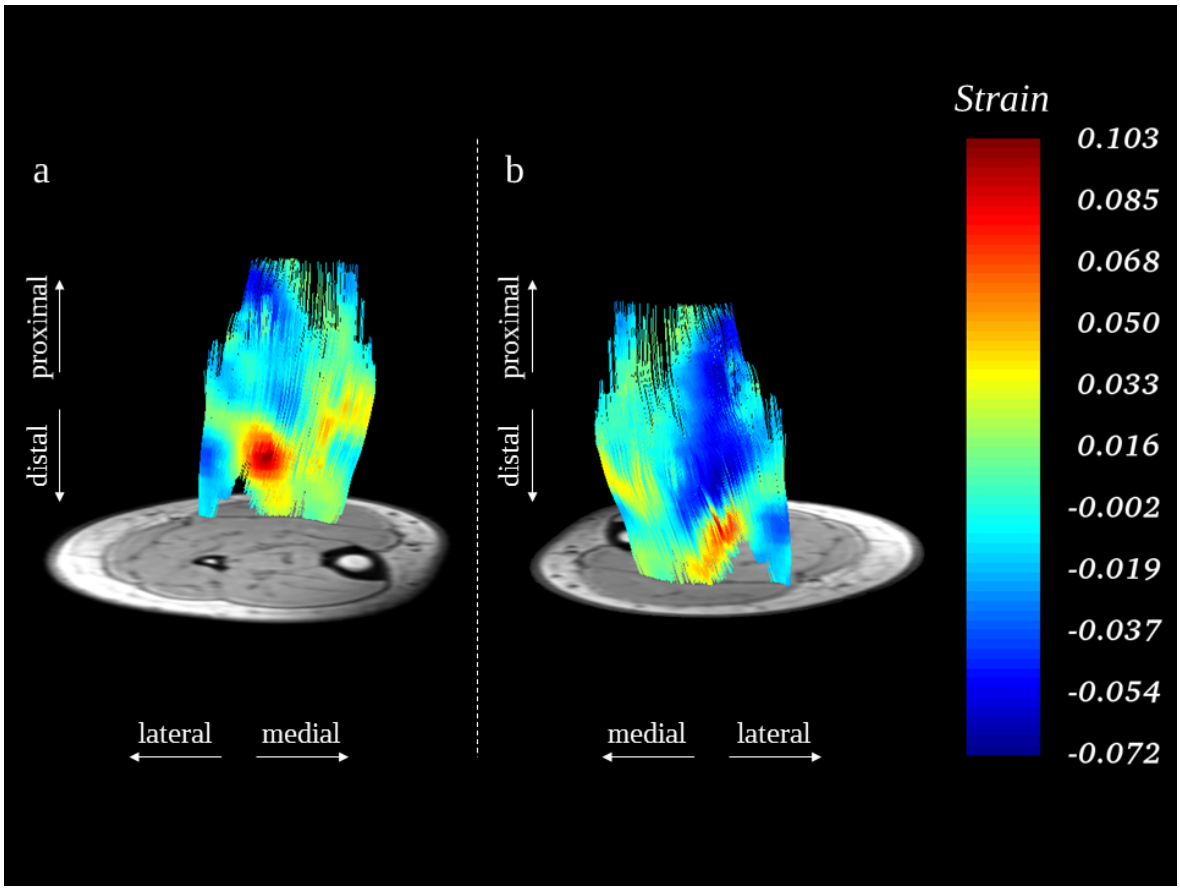

Figure 3.4 3D visualization of the reconstructed GM tracts for Subject-C. Tracts are color coded to represent deformation strain measured due to transition from 15% MVC to 5% MVC isometric plantar flexion. (a) Anterior-lateral view. (b) Posterior-medial view. Colorbar enumerates fiber direction strain presented on the tracts. Positive strain indicates lengthening, negative strain indicates shortening w.r.t. undeformed state.

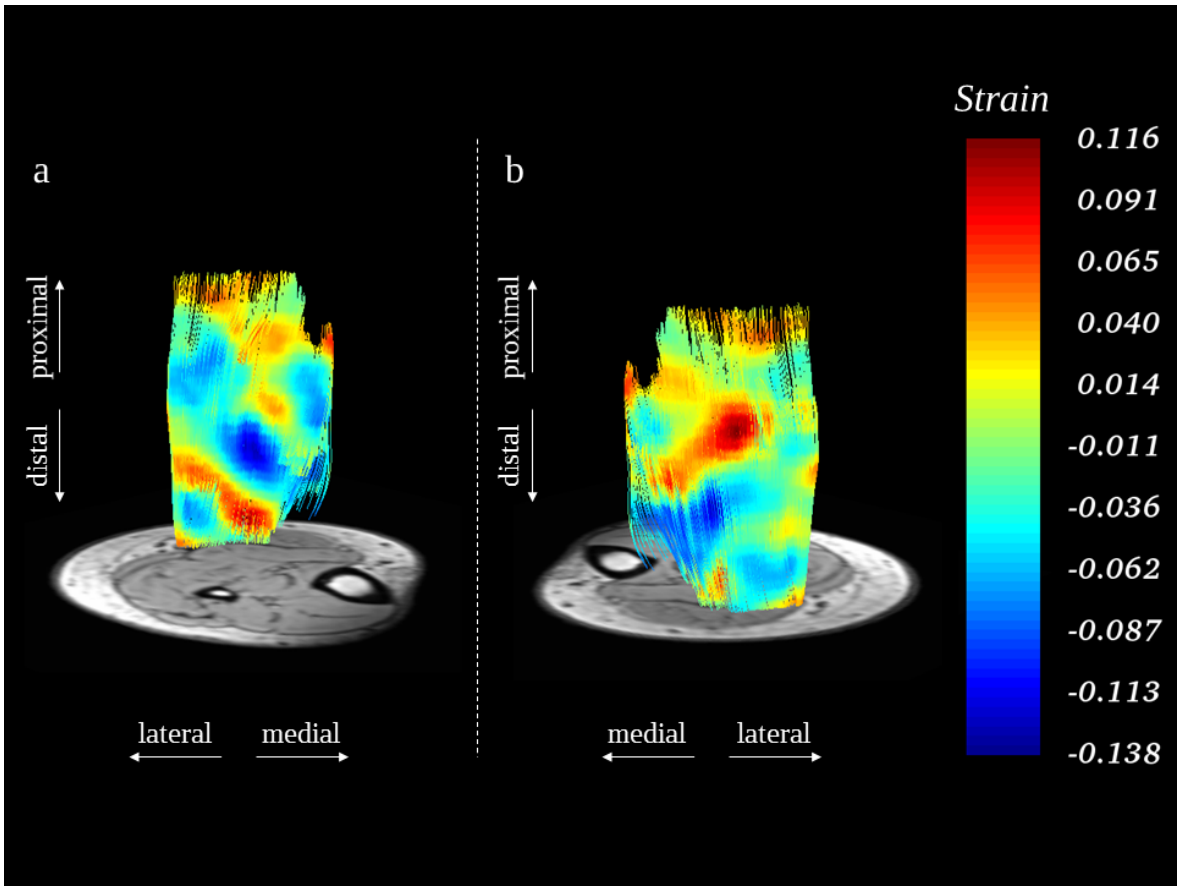

Figure 3.5 3D visualization of the reconstructed GM tracts for Subject-D. Tracts are color coded to represent deformation strain measured due to transition from 15% MVC to 5% MVC isometric plantar flexion. (a) Anterior-lateral view. (b) Posterior-medial view. Colorbar enumerates fiber direction strain presented on the tracts. Positive strain indicates lengthening, negative strain indicates shortening w.r.t. undeformed state.

3.2 Mean Fiber Direction Strain

Mean fiber strain distributions show variability. For Subject-A (Figure 3.6) and Subject-D (Figure 3.9) on average, the medial tracts shortened (by up to 3.1% for Subject-A and 4.6% for Subject-D), whereas the lateral tracts lengthened (by up to 5.2% for Subject-A and 0.3% for Subject-D). For Subject-C (Figure 3.8) the picture is completely reversed; that is, the medial tracts lengthened(by up to 2.1%), the lateral tracts shortened (by up to 2.3%). Finally, for Subject-B (Figure 3.7) lengthening and shortening are relatively evenly distributed (by 0.5% and 3.8%, respectively). For that subject, the lengthened muscle fibers are only slightly more populous toward the medial portion of the GM.

Presented results confirm the hypothesis that altering the level of activation during sustained isometric low-level plantar flexion causes simultaneous length changes along the muscle fibers of the human GM.

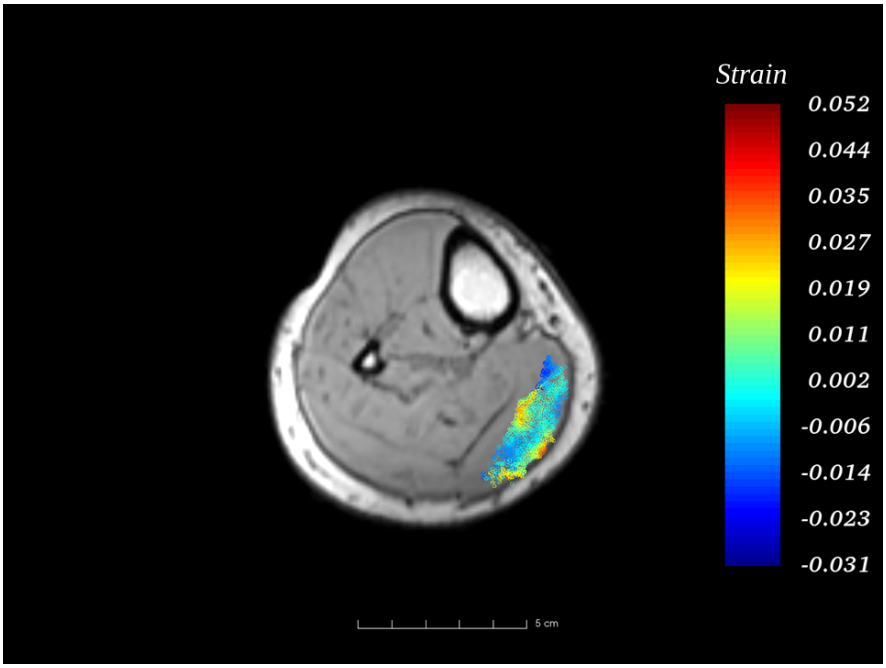

Figure 3.6 Mean length change of each fiber for Subject-A. Colorbar enumerates mean fiber direction strain presented on the tracts. Positive strain indicates lengthening, negative strain indicates shortening w.r.t. undeformed state.

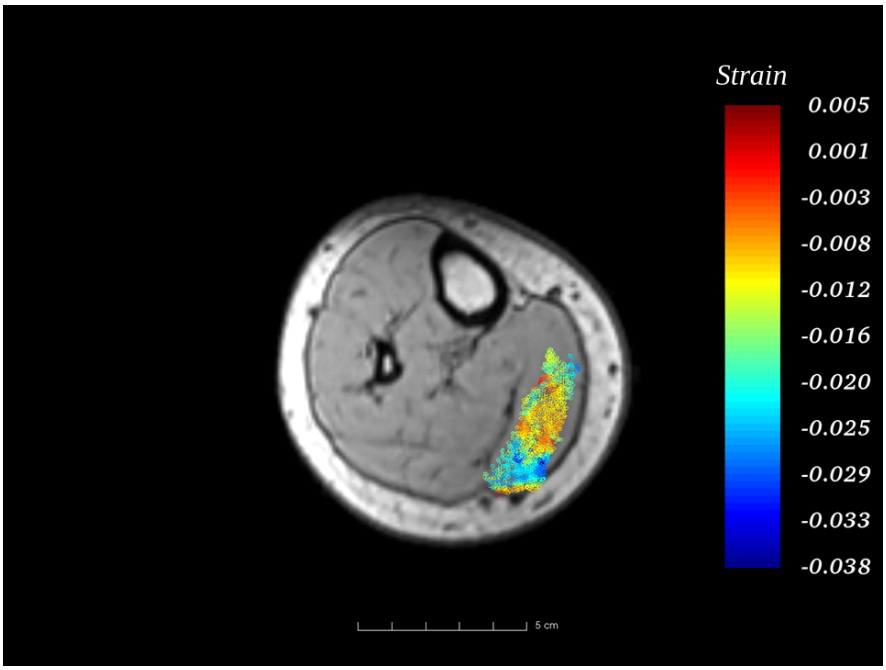

Figure 3.7 Mean length change of each fiber for Subject-B. Colorbar enumerates mean fiber direction strain presented on the tracts. Positive strain indicates lengthening, negative strain indicates shortening w.r.t. undeformed state.

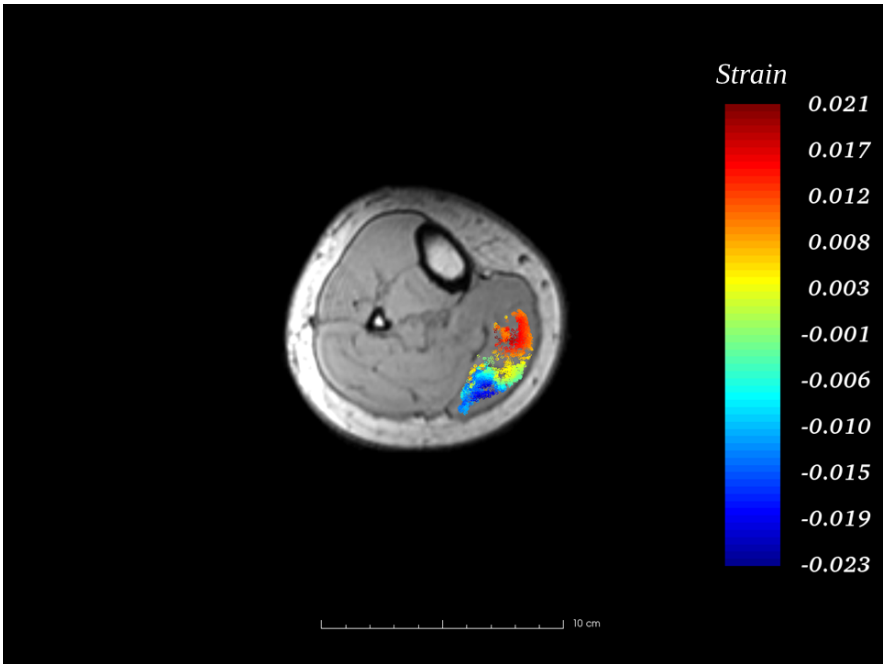

Figure 3.8 Mean length change of each fiber for Subject-C. Colorbar enumerates mean fiber direction strain presented on the tracts. Positive strain indicates lengthening, negative strain indicates shortening w.r.t. undeformed state.

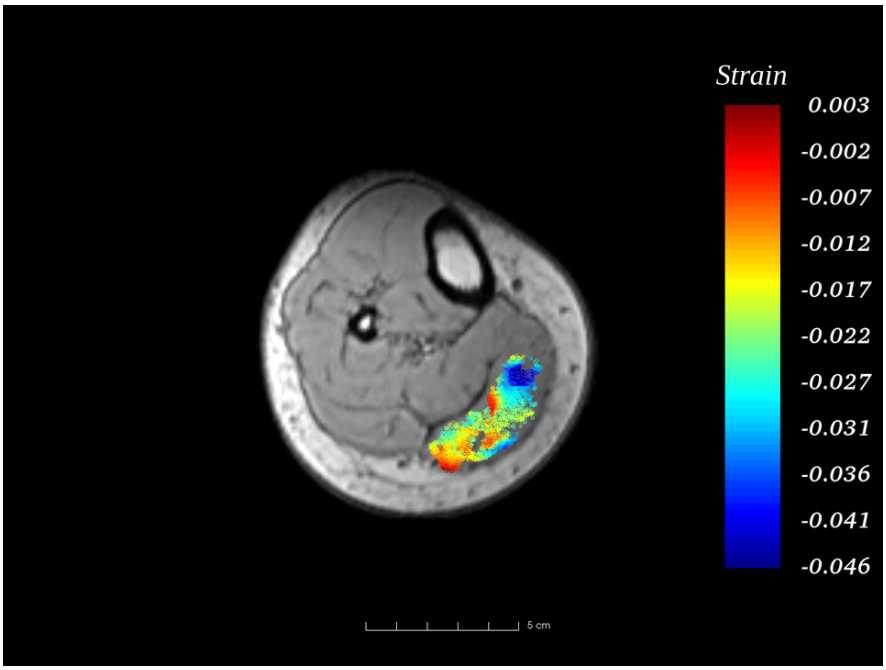

Figure 3.9 Mean length change of each fiber for Subject-D. Colorbar enumerates mean fiber direction strain presented on the tracts. Positive strain indicates lengthening, negative strain indicates shortening w.r.t. undeformed state.

4. DISCUSSION

This study aimed to observe the length changes that occur inside the skeletal muscle and along the muscle fibers during a change in activity. To this end, the GM muscle was imaged performing sustained isometric contractions varying from 15% to 5% MVC. We collected detailed anatomical images and DTI data, then processed the raw data to get strain and fiber directionality information. Distribution of local muscle fiber direction length changes were observed to be inhomogeneous in response to the tested change in muscular activity. Previous studies have shown similar results (e.g., [38, 17]), however they were not combined with muscular tract information in order to approximate length changes along muscle fibers. In this study, this method guided the experimentation, data analyses, and visualization. This in turn, allowed observing how strain is distributed in series along and laterally among muscle fiber tracts. Two important methods were key to obtain results in this study: fiber tractography through DTI, strain analysis through demons image registration and correlating data from these two sources (by vector mathematics). The methodology developed is unique and assessment of fiber direction strain distributions resulting from muscle activation change is novel.

There have been two main approaches in attempting to detect local tissue deformations *in vivo*. First is the direct method utilizing cardiac sequences such as Cine phase contrast (PC) [38, 17], spatial tagging [39], displacement encoding with stimulated echoes (DENSE) [40, 41] to track mobile tissue in repetitive motion. Second approach is to use non-rigid image registration as a post-processing step to infer the changes between two static states. Demons registration method has been previously utilized to study the effects of knee angle change [42, 5], application of kinesiotape [43] on the muscles of the lower leg. Registration method also was used combined with muscle fiber tractography to study knee angle change [19], and plantar flexion activity [44].

When using a direct method for strain detection, rapid repetition between desired states is a necessity. To achieve detection tissues need to be dynamic because magnetically tagged muscle tissue loses useful coherence in the order of a second [45]. Isometric contractions were studied by having subjects perform consecutive contractions in fast succession. For instance Kinugasa et al. [17] studied GM aponeurosis in isometric conditions under 64 contractions per minute. Image registration method, in contrast, allows for persistent change without time limitations. Study of conditions such as sustained isometric plantar flexion activity requires this property.

Earlier finite element modeling studies showed that muscular activity causes simultaneous lengthening and shortening along the same fibers, theoretically [15, 46]. The results were achieved by treating intracellular domain and ECM domain of skeletal muscle as elastically connected separate entities. Interaction between active elements and ECM modifies the length-force characteristics of the muscle in different contexts. Renewed understanding has implications on surgical interventions such as aponeurotomy [16, 47], botulinum toxin treatment [48, 49].

Existence of epimuscular interactions have previously been shown [14, 50, 51]. This relies on connective tissue structures such as collagen reinforced neurovascular tracts that interconnect neighboring muscles in the same compartment as well as distant muscles in different compartments. On joint position changes relative positions of these muscles change with respect to each other and this stretches connective tissue structures and leads to myofascial loads to act on the muscle bellies. Changes in muscle activity can also affect these loads.

A consequence of myofascial loads is that they affect deformation of muscle tissue and cause variations of that within the muscle belly. This has a component along the muscle fibers as well and leads to heterogeneously distributed lengthening and shortening along the same muscle fibers. Neighboring muscles such as SOL and GM places share epimuscular connections that are capable of imposing deformation when the relative position between the pair changes. Pamuk et al. [19] observed proximal lengthening combined with distal shortening on GM when knee extension

was imposed, alluding to SOL connections stretching to apply a distal force on GM muscle belly. While carrying such myofascial loads, epimuscular connections' ability to act as force transmission pathways during muscle activity also alters [52].

Karakuzu et al. [44] attributed their results showing a general pattern of distal lengthening and proximal shortening to neurovascular tracts carrying force generated by SOL to GM. In that work, the authors visualized key neurovascular tracts and quantified principal strains along those structures. This indicates that the neurovascular tracts are indeed exposed to myofascial loads and that they can transmit those into the muscle belly. Karakuzu et al. [44] showed that local high stretches along the muscle fascicles are concentrated in locations where the neurovascular tracts enter into the GM.

The results show that fibers are simultaneously lengthened and shortened along their length. Presence of variance in length changes were previously shown in *in vitro* animal studies [8] and model studies [15, 53]. At first glance this result can be counter-intuitive because fibers are activated along their entire length. Such an argument overlooks or underestimates the effect of connective tissues on muscle's operation. When the non-uniform interaction with the fascia as a function of position is taken into consideration, one can make sense of this result.

Individual variability on the strength and elasticity of mechanical connections between GM and SOL is not well studied. While it is difficult to point to a general pattern, lengthening in distal part of GM was a shared property among subjects. It can therefore be said that, distal lengthening was increased with decreased muscular activity. Amount of changes in length were relatively low, with a maximum of 32.7% in Subject-A, compared to 108% strain observed as a result of transition from passive condition to 15% MVC contraction of GM [44]. Global GM movement in proximal direction relative to SOL, due to plantar flexion activity was previously observed [17]. Amount of movement was proportional to the amount of contraction. Decrease of contraction therefore must have resulted GM moving to a more distal position and altering the myofascial loads bearing on the muscle belly in a non-uniform fashion.

Muscle recruitment strategies were found to differ during both dynamic exercises [54], and varying levels of isometric activity [55]. This mechanism might also explain the somewhat checkered distribution of fiber direction length changes on the GM. When the level of contraction changed, muscle recruitment strategies employed by the subjects during the imaging must have necessarily altered. Subjects may have produced the required force by utilizing a different population of fibers. Yet, interaction of muscle and the fascia will change on decreased muscle activation such that myofascial loads acting on the GM in the present work must differ compared to the previous study testing 15% MVC [44] both in terms of amplitude and direction. Changing sarcomere lengths in the two configurations can be explained as a result of such variation.

Ateş et al. [56, 57] intraoperative studies on human spastic muscle has shown the significance of MFT in a clinical setting. Also, effects of administering botulinum toxin type A (BTX-A) were examined through *in situ* animal studies [58, 59] and finite element model studies [48, 49]. Medical practitioners can glean information on mechanical state of the patient prior to an intervention through the means this study was conducted. And, once an operation has gone underway, ability to gather data, *in vivo* will remain useful for monitoring muscle tissues' progress; and ultimately be useful in assessing the utility of the operation.

Improved understanding of mechanics further can be applied on injuries as well as pathologies(e.g.[40]). Human studies regarding mechanical effects of BTX-A, *in vivo* is lacking. Application of this methodology also presents a research opportunity in this area. This study can be extended to inspect mechanical interactions between synergistic muscles (e.g. GAS, SOL) and antagonists. Currently, a technical limitation in DTI image acquisition – ghosting of fat tissue overlapping with muscle tissue partially – prevents the completion of such study.

5. CONCLUSION

The present findings show simultaneous lengthening and shortening along GM muscle fibers, as well as among them. Despite the resolution limitations due to the imaging modality, these results allude to serial and parallel sarcomere length heterogeneity. Variance in sarcomere length changes has been linked to muscle's range of force exertion capability [60]. Also, heterogeneity in the parallel strain distribution was indicated to extend the optimal muscle length [61]. Finite element modeling studies revealed the mechanisms behind those findings for healthy muscles [46, 52], as well as for pathological muscles undergoing interventions [47, 62]. Present study offers practical evidence for the validity of the modeling studies. Thus, the methodology used in this study can be applied as a tool for evaluating changes in the range of motion in human muscles. Range of motion is hindered in the atrophied muscles. Methods of this study can be applied to evaluate the effectiveness common interventions (e.g. botulinum toxin treatment, aponeurotomy), and perhaps guide practitioners' course of action.

In conclusion, advanced MRI and DTI techniques were combined to generate a method capable of analyzing length changes in the muscle fiber direction. Study of varying muscular activity revealed sizable distribution of strain along human GM muscle fibers, *in vivo*.

REFERENCES

1. Richfield, D., "Medical gallery of david richfield," *WikiJournal of Medicine*, Vol. 1, no. 2, 2014.

2. "Muscles," *Northampton Community Collage*, Accessed May 25, 2017, https://www.studyblue.com/notes/note/n/muscles/deck/18324329.

3. Sobotta, J., *Sobotta's Atlas and Text-book of Human Anatomy*, 1909.

4. Braus, H., *Anatomie des Menschen: ein Lehrbuch für Studierende und Ärzte*, 1921.

5. Yaman, A., C. Ozturk, P. A. Huijing, and C. A. Yucesoy, "Magnetic resonance imaging assessment of mechanical interactions between human lower leg muscles in vivo," *Journal of Biomechanical Engineering*, Vol. 135, no. 9, pp. 091003–091003, 2013.

6. Huxley, H., and J. Hanson, "Changes in the cross-striations of muscle during contraction and stretch and their structural interpretation," *Nature*, Vol. 173, pp. 973–976, 1954.

7. Huxley, A. F., and R. Niedergerke, "Structural changes in muscle during contraction; interference microscopy of living muscle fibres.," *Nature*, Vol. 173, no. 4412, pp. 971–973, 1954.

8. Street, S. F., "Lateral transmission of tension in frog myofibers: A myofibrillar network and transverse cytoskeletal connections are possible transmitters," *Journal of Cellular Physiology*, Vol. 114, no. 3, pp. 346–364, 1983.

9. Trotter, J., and P. Purslow, "Functional morphology of the endomysium in series fibered muscles," *Journal of Morphology*, Vol. 212, no. 2, pp. 109–122, 1992.

10. Huijing, P. A., "Muscle as a collagen fiber reinforced composite: a review of force transmission in muscle and whole limb," *Journal of Biomechanics*, Vol. 32, no. 4, pp. 329 – 345, 1999.

11. Maas, H., G. C. Baan, and P. A. Huijing, "Intermuscular interaction via myofascial force transmission: effects of tibialis anterior and extensor hallucis longus length on force transmission from rat extensor digitorum longus muscle," *Journal of biomechanics*, Vol. 34, no. 7, pp. 927–940, 2001.

12. Huijing, P. A., and G. C. Baan, "Myofascial force transmission: muscle relative position and length determine agonist and synergist muscle force," *Journal of Applied Physiology*, Vol. 94, no. 3, pp. 1092–1107, 2003.

13. Maas, H., G. C. Baan, and P. A. Huijing, "Muscle force is determined also by muscle relative position: isolated effects," *Journal of biomechanics*, Vol. 37, no. 1, pp. 99–110, 2004.

14. Yucesoy, C. A., G. C. Baan, B. H. Koopman, H. J. Grootenboer, and P. A. Huijing, "Pre-strained epimuscular connections cause muscular myofascial force transmission to affect properties of synergistic ehl and edl muscles of the rat," *Journal of biomechanical engineering*, Vol. 127, no. 5, pp. 819–828, 2005.

15. Yucesoy, C. A., B. H. Koopman, P. A. Huijing, and H. J. Grootenboer, "Three-dimensional finite element modeling of skeletal muscle using a two-domain approach: linked fiber-matrix mesh model," *Journal of biomechanics*, Vol. 35, no. 9, pp. 1253–1262, 2002.

16. Yucesoy, C. A., and P. A. Huijing, "Substantial effects of epimuscular myofascial force transmission on muscular mechanics have major implications on spastic muscle and remedial surgery," *Journal of Electromyography and Kinesiology*, Vol. 17, no. 6, pp. 664–679, 2007.

17. Kinugasa, R., D. Shin, J. Yamauchi, C. Mishra, J. A. Hodgson, V. R. Edgerton, and S. Sinha, "Phase-contrast mri reveals mechanical behavior of superficial and deep aponeuroses in human medial gastrocnemius during isometric contraction," *Journal of Applied Physiology*, Vol. 105, no. 4, pp. 1312–1320, 2008.

18. Thirion, J.-P., "Image matching as a diffusion process: an analogy with maxwell's demons," *Medical image analysis*, Vol. 2, no. 3, pp. 243–260, 1998.

19. Pamuk, U., A. Karakuzu, C. Ozturk, B. Acar, and C. A. Yucesoy, "Combined magnetic resonance and diffusion tensor imaging analyses provide a powerful tool for in vivo assessment of deformation along human muscle fibers," *Journal of the Mechanical Behavior of Biomedical Materials*, Vol. 63, pp. 207 – 219, 2016.

20. Damon, B. M., "Effects of image noise in muscle diffusion tensor (dt)-mri assessed using numerical simulations," *Magnetic Resonance in Medicine*, Vol. 60, no. 4, pp. 934–944, 2008.

21. Heemskerk, A. M., T. K. Sinha, K. J. Wilson, Z. Ding, and B. M. Damon, "Quantitative assessment of dti-based muscle fiber tracking and optimal tracking parameters," *Magnetic Resonance in Medicine*, Vol. 61, no. 2, pp. 467–472, 2009.

22. Holl, N., A. Echaniz-Laguna, G. Bierry, M. Mohr, J.-P. Loeffler, T. Moser, J.-L. Dietemann, and S. Kremer, "Diffusion-weighted mri of denervated muscle: a clinical and experimental study," *Skeletal Radiology*, Vol. 37, no. 12, pp. 1111–1117, 2008.

23. Neji, R., G. Langs, J. F. Deux, M. Maatouk, A. Rahmouni, G. Bassez, G. Fleury, and N. Paragios, "Unsupervised classification of skeletal fibers using diffusion maps," in *2009 IEEE International Symposium on Biomedical Imaging: From Nano to Macro*, pp. 410–413, June 2009.

24. Saupe, N., L. M. White, J. Stainsby, G. Tomlinson, and M. S. Sussman, "Diffusion tensor imaging and fiber tractography of skeletal muscle: Optimization of b value for imaging at 1.5 t," *American Journal of Roentgenology*, Vol. 192, pp. W282–W290, Jun 2009.

25. Henkelman, R. M., "Measurement of signal intensities in the presence of noise in mr images," *Medical Physics*, Vol. 12, no. 2, pp. 232–233, 1985.

26. Basser, P. J., S. Pajevic, C. Pierpaoli, J. Duda, and A. Aldroubi, "In vivo fiber tractography using dt-mri data," *Magnetic resonance in medicine*, Vol. 44, no. 4, pp. 625–632, 2000.

27. Tristán-Vega, A., and S. Aja-Fernández, "Dwi filtering using joint information for dti and hardi," *Medical Image Analysis*, Vol. 14, no. 2, pp. 205–218, 2010.

28. Clarke, R. A., P. Scifo, G. Rizzo, F. Dell'Acqua, G. Scotti, and F. Fazio, "Noise correction on rician distributed data for fibre orientation estimators," *IEEE transactions on Medical Imaging*, Vol. 27, no. 9, pp. 1242–1251, 2008.

29. Aja-Fernández, S., C. Alberola-López, and C.-F. Westin, "Noise and signal estimation in magnitude mri and rician distributed images: a lmmse approach," *IEEE transactions on image processing*, Vol. 17, no. 8, pp. 1383–1398, 2008.

30. Yoldemir, A. B., "Assessing dt-mri tractography results via sampling the fiber tract space," Master's thesis, Electrical and Electronics Engineering, Bogazici University, 2011.

31. Durusut, E., U. Bozkaya, E. Yagci, and B. Acar, "Vavframe: A new concept in platform design," in *EUROCON 2005-The International Conference on" Computer as a Tool"*, Vol. 1, pp. 370–373, IEEE, 2005.

32. Froeling, M., A. J. Nederveen, D. F. Heijtel, A. Lataster, C. Bos, K. Nicolay, M. Maas, M. R. Drost, and G. J. Strijkers, "Diffusion-tensor mri reveals the complex muscle architecture of the human forearm," *Journal of Magnetic Resonance Imaging*, Vol. 36, no. 1, pp. 237–248, 2012.

33. Descoteaux, M., R. Deriche, T. R. Knosche, and A. Anwander, "Deterministic and probabilistic tractography based on complex fibre orientation distributions," *IEEE transactions on medical imaging*, Vol. 28, no. 2, pp. 269–286, 2009.

34. Chow, R., M. Medri, D. Martin, R. Leekam, A. Agur, and N. McKee, "Sonographic studies of human soleus and gastrocnemius muscle architecture: gender variability," *European journal of applied physiology*, Vol. 82, no. 3, pp. 236–244, 2000.

35. Tench, C., P. Morgan, M. Wilson, and L. Blumhardt, "White matter mapping using diffusion tensor mri," *Magnetic Resonance in Medicine*, Vol. 47, no. 5, pp. 967–972, 2002.

36. Akyazı, P., "Skeletal muscle deformation analysis using di?usion tensor magnetic resonance imaging," Master's thesis, Bogazici University, Istanbul, Turkey, 2013.

37. Fedorov, A., R. Beichel, J. Kalpathy-Cramer, J. Finet, J.-C. Fillion-Robin, S. Pujol, C. Bauer, D. Jennings, F. Fennessy, M. Sonka, J. Buatti, S. Aylward, J. V. Miller, S. Pieper, and R. Kikinis, "3d slicer as an image computing platform for the quantitative imaging network," *Magnetic Resonance Imaging*, Vol. 30, no. 9, pp. 1323 – 1341, 2012. Quantitative Imaging in Cancer.

38. Pappas, G. P., D. S. Asakawa, S. L. Delp, F. E. Zajac, and J. E. Drace, "Nonuniform shortening in the biceps brachii during elbow flexion," *Journal of Applied Physiology*, Vol. 92, no. 6, pp. 2381–2389, 2002.

39. Englund, E. K., C. P. Elder, Q. Xu, Z. Ding, and B. M. Damon, "Combined diffusion and strain tensor mri reveals a heterogeneous, planar pattern of strain development during isometric muscle contraction," *American Journal of Physiology - Regulatory, Integrative and Comparative Physiology*, Vol. 300, no. 5, pp. R1079–R1090, 2011.

40. Fiorentino, N. M., F. H. Epstein, and S. S. Blemker, "Activation and aponeurosis morphology affect *in vivo* muscle tissue strains near the myotendinous junction," *Journal of Biomechanics*, Vol. 45, no. 4, pp. 647–652, 2011.

41. Zhong, X., F. H. Epstein, B. S. Spottiswoode, and S. S. Blemker, "Imaging two-dimensional displacements and strains in skeletal muscle during joint motion by cine dense mr," *Journal of Biomechanics*, Vol. 41, no. 3, pp. 532–540, 2008.

42. Huijing, P. A., A. Yaman, C. Ozturk, and C. A. Yucesoy, "Effects of knee joint angle on global and local strains within human triceps surae muscle: Mri analysis indicating in vivo myofascial force transmission between synergistic muscles," *Surgical and Radiologic Anatomy*, Vol. 33, no. 10, pp. 869–879, 2011.

43. Pamuk, U., and C. A. Yucesoy, "{MRI} analyses show that kinesio taping affects much more than just the targeted superficial tissues and causes heterogeneous deformations within the whole limb," *Journal of Biomechanics*, Vol. 48, no. 16, pp. 4262 – 4270, 2015.

44. Karakuzu, A., U. Pamuk, C. Ozturk, B. Acar, and C. A. Yucesoy, "Magnetic resonance and diffusion tensor imaging analyses indicate heterogeneous strains along human medial gastrocnemius fascicles caused by submaximal plantar-flexion activity," *Journal of Biomechanics*, 2017/05/06 2017.

45. Fleckenstein, J., R. Canby, R. Parkey, and R. Peshock, "Acute effects of exercise on mr imaging of skeletal muscle in normal volunteers," *American Journal of Roentgenology*, Vol. 151, no. 2, pp. 231–237, 1988.

46. Yucesoy, C. A., and P. A. Huijing, "Specifically tailored use of the finite element method to study muscular mechanics within the context of fascial integrity: the linked fiber-matrix mesh model," *International Journal for Multiscale Computational Engineering*, Vol. 10, no. 2, pp. 155–170, 2012.

47. Yucesoy, C. A., and P. A. Huijing, "Assessment by finite element modeling indicates that surgical intramuscular aponeurotomy performed closer to the tendon enhances intended acute effects in extramuscularly connected muscle," *Journal of Biomechanical Engineering*, Vol. 131, pp. 021012–021012–9, Dec 2008.

48. Turkoglu, A. N., P. A. Huijing, and C. A. Yucesoy, "Mechanical principles of effects of botulinum toxin on muscle length-force characteristics: An assessment by finite element modeling," *Journal of Biomechanics*, Vol. 47, no. 7, pp. 1565 – 1571, 2014.

49. Turkoglu, A. N., and C. A. Yucesoy, "Simulation of effects of botulinum toxin on muscular mechanics in time course of treatment based on adverse extracellular matrix adaptations," *Journal of Biomechanics*, Vol. 49, no. 7, pp. 1192 – 1198, 2016.

50. Yucesoy, C. A., B. H. F. J. M. Koopman, H. J. Grootenboer, and P. A. Huijing, "Extramuscular myofascial force transmission alters substantially the acute effects of surgical aponeurotomy: assessment by finite element modeling," *Biomechanics and Modeling in Mechanobiology*, Vol. 7, no. 3, pp. 175–189, 2008.

51. Yucesoy, C. A., "Epimuscular myofascial force transmission implies novel principles for muscular mechanics," *Exercise & Sport Sciences Reviews*, Vol. 38, no. 3, pp. 128–134, 2010.

52. Yucesoy, C. A., B. H. Koopman, G. C. Baan, H. J. Grootenboer, and P. A. Huijing, "Effects of inter- and extramuscular myofascial force transmission on adjacent synergistic muscles: assessment by experiments and finite-element modeling," *Journal of Biomechanics*, Vol. 36, no. 12, pp. 1797–1811, 2003.

53. Blemker, S. S., P. M. Pinsky, and S. L. Delp, "A 3d model of muscle reveals the causes of nonuniform strains in the biceps brachii," *Journal of Biomechanics*, Vol. 38, no. 4, pp. 657–665, 2005.

54. Hodson-Tole, E. F., and J. M. Wakeling, "Motor unit recruitment for dynamic tasks: current understanding and future directions," *Journal of Comparative Physiology B*, Vol. 179, no. 1, pp. 57–66, 2009.

55. Kinugasa, R., Y. Kawakami, S. Sinha, and T. Fukunaga, "Unique spatial distribution of in vivo human muscle activation," *Experimental Physiology*, Vol. 96, no. 9, pp. 938–948, 2011.

56. Ateş, F., Y. Temelli, and C. A. Yucesoy, "Human spastic gracilis muscle isometric forces measured intraoperatively as a function of knee angle show no abnormal muscular mechanics," *Clinical Biomechanics*, Vol. 28, no. 1, pp. 48 – 54, 2013.

57. Ateş, F., Y. Temelli, and C. A. Yucesoy, "Intraoperative experiments show relevance of inter-antagonistic mechanical interaction for spastic muscle's contribution to joint movement disorder," *Clinical Biomechanics*, Vol. 29, no. 8, pp. 943–949, 2014.

58. Ateş, F., and C. A. Yucesoy, "Effects of botulinum toxin type a on non-injected biarticular muscle include a narrower length range of force exertion and increased passive force," *Muscle & Nerve*, Vol. 49, no. 6, pp. 866–878, 2014.

59. Yucesoy, C. A., A. N. Turkoğlu, S. Umur, and F. Ateş, "Intact muscle compartment exposed to botulinum toxin type a shows compromised intermuscular mechanical interaction," *Muscle & Nerve*, Vol. 51, no. 1, pp. 106–116, 2015.

60. Morgan, D. L., N. P. Whitehead, A. K. Wise, J. E. Gregory, and U. Proske, "Tension changes in the cat soleus muscle following slow stretch or shortening of the contracting muscle," *The Journal of Physiology*, Vol. 522, no. 3, pp. 503–513, 2000.

61. Willems, M. E. T., and P. A. Huijing, "Heterogeneity of mean sarcomere length in different fibres: effects on length range of active force production in rat muscle," *European Journal of Applied Physiology and Occupational Physiology*, Vol. 68, no. 6, pp. 489–496, 1994.

62. Yucesoy, C. A., prof.dr.ir. Bart H.F.J.M. Koopman, prof.dr.ir. Henk J. Grootenboer, and prof.dr. Peter A. Huijing, "Finite element modeling of aponeurotomy: altered intramuscular myofascial force transmission yields complex sarcomere length distributions determining acute effects," *Biomechanics and modeling in mechanobiology*, Vol. 6, no. 4, pp. 227–243, 2007.